

Optical properties of the iron-arsenic superconductor $\text{BaFe}_{1.85}\text{Co}_{0.15}\text{As}_2$

J. J. Tu, J. Li, W. Liu, and A. Punnoose

Department of Physics, The City College of New York, New York, NY 10031

Y. Gong and Y. H. Ren

Department of Physics and Astronomy, Hunter College of the City University of New York, New York, NY 10065

L. J. Li, G. H. Cao, and Z. A. Xu

Department of Physics, Zhejiang University, Hangzhou 310027, China

C. C. Homes*

*Department of Condensed Matter Physics and Materials Science,
Brookhaven National Laboratory, Upton, NY 11973*

(Dated: August 9, 2018)

The transport and complex optical properties of the electron-doped iron-arsenic superconductor $\text{BaFe}_{1.85}\text{Co}_{0.15}\text{As}_2$ with $T_c = 25$ K have been examined in the Fe-As planes above and below T_c . A Bloch-Grüneisen analysis of the resistivity yields a weak electron-phonon coupling constant $\lambda_{ph} \simeq 0.2$. The low-frequency optical response in the normal state appears to be dominated by the electron pocket and may be described by a weakly-interacting Fermi liquid with a Drude plasma frequency of $\omega_{p,D} \simeq 7840 \text{ cm}^{-1}$ ($\simeq 0.972 \text{ eV}$) and scattering rate $1/\tau_D \simeq 126 \text{ cm}^{-1}$ ($\simeq 15 \text{ meV}$) just above T_c . The frequency-dependent scattering rate $1/\tau(\omega)$ has kinks at $\simeq 12$ and 55 meV that appear to be related to bosonic excitations. Below T_c the majority of the superconducting plasma frequency originates from the electron pocket and is estimated to be $\omega_{p,S} \simeq 5200 \text{ cm}^{-1}$ ($\lambda_0 \simeq 3000 \text{ \AA}$) for $T \ll T_c$, indicating that less than half the free carriers in the normal state have collapsed into the condensate, suggesting that this material is not in the clean limit. Supporting this finding is the observation that this material falls close to the universal scaling line for a BCS dirty-limit superconductor in the weak-coupling limit. There are two energy scales for the superconductivity in the optical conductivity and photo-induced reflectivity at $\Delta_1(0) \simeq 3.1 \pm 0.2 \text{ meV}$ and $\Delta_2(0) \simeq 7.4 \pm 0.3 \text{ meV}$. This corresponds to either the gapping of the electron and hole pockets, respectively, or an anisotropic s -wave gap on the electron pocket; both views are consistent with the s^\pm model.

PACS numbers: 74.25.Gz, 74.70.Xa, 78.30.-j

I. INTRODUCTION

Since its discovery nearly a century ago, the field of superconductivity has periodically reinvented itself. A significant advance in the understanding of this phenomenon was achieved through the model by Bardeen, Cooper and Schrieffer (BCS), which proposed that below a critical temperature T_c electrons condense into pairs which are coupled through lattice vibrations;¹ these so-called Cooper pairs are bosons which constitute a supercurrent that may flow without loss. Below T_c an isotropic s -wave gap also opens in the spectrum of excitations across the Fermi surface. Within this model, it was thought that the T_c 's of conventional metals and alloys could not exceed $\simeq 30 \text{ K}$ (Ref. 2). The discovery of superconductivity at elevated temperatures in the copper-oxide materials³ with T_c 's in excess of 130 K at ambient pressure and an unusual d -wave superconducting energy gap⁴ indicates that these materials are not phonon mediated; indeed, the coupling mechanism in these materials remains unresolved and a subject of considerable debate. The discovery of superconductivity in MgB_2 with a surprisingly high transition temperature $T_c = 39 \text{ K}$ initially suggested an unusual pairing mechanism.⁵ However, the isotope effect firmly established that this mate-

rial is phonon mediated;⁶ in this case the high phonon frequencies in MgB_2 are likely responsible for the enhanced critical temperature.⁷

The recent discovery superconductivity in the iron-arsenic $\text{LaFeAsO}_{1-x}\text{F}_x$ (1111) compound⁸ at ambient pressure ($T_c = 26 \text{ K}$) was surprising because iron and magnetic impurities in general were considered detrimental to the formation of superconductivity; T_c 's $\gtrsim 50 \text{ K}$ in this material were quickly achieved through rare-earth substitutions.⁹⁻¹² While such high values for T_c do not necessarily rule out a phonon-mediated pairing mechanism, the close proximity of magnetic order and superconductivity in these compounds¹³ has led to the suggestion that the pairing in this class of materials may have another origin.¹⁴⁻¹⁷ While the highest T_c 's are observed in the 1111 compounds, large single crystals of these materials have proven difficult to grow. For this reason attention has shifted to the structurally-simpler BaFe_2As_2 (122) materials, where large single crystals are readily available. Unlike the cuprates, the parent compound is metallic with a structural and magnetic transition at $T_N \simeq 140 \text{ K}$, below which it remains metallic.¹⁸ The emergence of superconductivity and the suppression of the magnetic and structural transitions may be achieved through the application of pressure¹⁹ or through

chemical substitution;^{20–23} K-doping results in a hole-doped material with a maximum $T_c \simeq 38$ K, while Ni- and Co-doping result in electron-doped materials with a somewhat lower maximum $T_c \simeq 29$ K. The electron- and hole-doped materials have been the subject of numerous investigations, including thermodynamic and transport studies,^{21–35} angle-resolved photoemission^{36–45} (ARPES), Raman^{46–49} and optical studies.^{50–65} Several of these studies address the nature of the superconducting gaps, such as whether there are multiple gaps and whether the gaps contain nodes. The experimental picture is not clear. The isotope effect in these materials is also uncertain; while a large Fe isotope effect has been reported in BaFe_2As_2 and $\text{Ba}_{0.6}\text{K}_{0.4}\text{Fe}_2\text{As}_2$ polycrystals,⁶⁶ an inverse iron isotope effect has also been observed.⁶⁷

Despite the structural differences of the iron-arsenic compounds, the band structure of these materials is remarkably similar, with a minimal description consisting of a hole band (α) centered at the Γ point and an electron band (β) at the M point of the Brillouin zone.^{68–70} The mobilities are thought to be significantly higher in the electron bands.³⁰ Several theoretical models^{71–74} propose that below T_c superconducting s -wave energy gaps form on the electron and hole pockets, possibly with a sign change between them, the so-called s^\pm model. In the s^\pm model the gap on the electron pocket may be an extended s -wave with nodes on its Fermi surface;⁷⁵ it is possible that disorder may lift the nodes.⁷⁶

In this work the electron-doped $\text{BaFe}_{1.85}\text{Co}_{0.15}\text{As}_2$ superconductor ($T_c = 25$ K) has been examined using several different techniques. The temperature dependence of the ab -plane resistivity is analyzed using a simple Bloch-Grüneisen framework, yielding an upper-bound for the electron-phonon coupling constant of $\lambda_{ph} \simeq 0.2$. The complex optical properties in the iron-arsenic planes have been examined in the normal and superconducting states. In the normal state, the free carrier response is dominated by the electron pocket and may be described by a simple Drude-Lorentz model. In the generalized-Drude response for $T \simeq T_c$ the frequency-dependent scattering rate shows clear kinks at about $\simeq 12$ meV and 55 meV, suggesting scattering from bosonic excitations. Below T_c the formation of a condensate is observed; however, less than 50% of the free carriers condense, suggesting this material is not in the clean limit. Supporting this view is the observation that this material is observed to fall close to the universal scaling line for a BCS dirty-limit superconductor in the weak-coupling limit. In order to properly model the optical conductivity below T_c it is necessary to introduce two superconducting energy gaps at $\Delta_1(0) = 3.1 \pm 0.2$ meV and $\Delta_2(0) = 7.4 \pm 0.4$ meV. This corresponds to either the gapping of the electron and hole pockets, respectively, or the gapping of the electron pocket by an anisotropic s -wave gap; both results are consistent with the s^\pm model. The time evolution of the photoinduced reflectivity change in the superconducting state yields almost identical values for the gaps. These results indicate that there are two energy scales

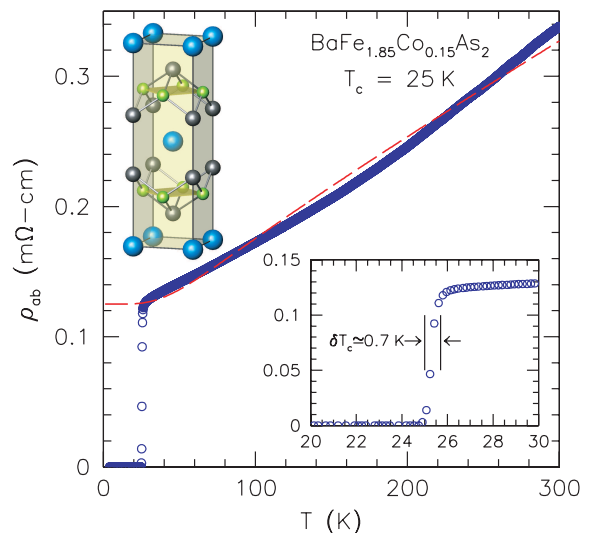


FIG. 1. Temperature dependent ab -plane resistivity of a $\text{BaFe}_{1.85}\text{Co}_{0.15}\text{As}_2$ single crystal with a superconducting transition at $T_c = 25$ K; the dashed curve is a Bloch-Grüneisen fit to the resistivity data (Sec. IIIC). Insets: The unit cell of BaFe_2As_2 in the tetragonal $I4/mmm$ setting; detail of the resistivity in the region of T_c illustrating the sharp transition width $\delta T_c \simeq 0.7$ K.

for the superconductivity in $\text{BaFe}_{1.85}\text{Co}_{0.15}\text{As}_2$ and that the pairing is likely not phonon mediated.

II. EXPERIMENT

Large single crystals of the iron-arsenic superconductor $\text{BaFe}_{2-x}\text{Co}_x\text{As}_2$ were grown by a self-flux method.²³ Energy dispersive x-ray (EDX) microanalysis was used to determine that the Co concentration $x = 0.15$ was at the optimal level. The resistivity in the ab -planes was measured using a standard four-probe method. The temperature dependence of the resistivity of a single crystal of $\text{BaFe}_{1.85}\text{Co}_{0.15}\text{As}_2$ is shown in Fig. 1; the resistivity displays a slight curvature before abruptly going to zero at $T_c \simeq 25$ K, with a transition width of less than 0.7 K (inset of Fig. 1). The temperature-dependent reflectance was measured at a near-normal angle of incidence from $\simeq 20$ to over 25,000 cm^{-1} ($\simeq 2$ meV to 3 eV) on a cleaved surface for light polarized in the ab -planes using *in situ* evaporation technique.⁷⁷ This large frequency interval is needed to carry out a reliable Kramers-Kronig analysis where extrapolations are supplied in the limits for $\omega \rightarrow 0, \infty$. For the transient reflectivity measurements, a Ti:sapphire laser system which can deliver 100-fs short pulses at an 80-MHz repetition rate, tunable at 800 nm (1.55 eV), was used as the source of both pump and probe pulses. A standard pump-probe setup is employed with the pump beam having a spot-diameter of 60 μm and the time-delayed probe beam with spot-diameter of 30 μm . The pump beam was modulated at 2 kHz with an optical

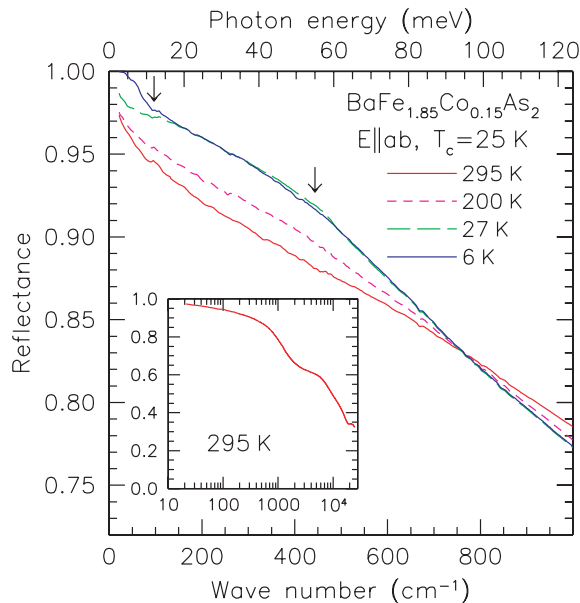


FIG. 2. The temperature dependence of the reflectance of single-crystal $\text{BaFe}_{1.85}\text{Co}_{0.15}\text{As}_2$ for light polarized in the a - b planes at several temperatures above and below T_c . There is a dramatic change in the reflectance below T_c . The kinks in low-temperature normal-state reflectivity (27 K) at ≈ 12 and 55 meV (marked by the two arrows at the inflection points in reflectivity) result from strong scattering of the carriers with some underlying bosonic excitations at these energy scales. Inset: The reflectance over a wide frequency range at 295 K.

chopper and a lock-in amplifier was used to measure the transient reflectivity change, $\Delta R/R$, of the probe beam.

III. RESULTS AND DISCUSSION

A. Optical properties

1. Normal state

The temperature dependence of the reflectance of $\text{BaFe}_{1.85}\text{Co}_{0.15}\text{As}_2$ for light polarized in the ab -planes is shown in the infrared region in Fig. 2 for several temperatures above and below T_c ; the reflectance at 295 K is shown over a much larger region in the inset. In the normal state, the reflectance at low frequency has a $R \propto 1 - \sqrt{\omega}$ response characteristic of a metal in the Hagen-Rubens regime. In addition to this generic response, just above T_c at 27 K there are two inflection points in the reflectance (indicated by arrows) at ≈ 12 and 55 meV, which may result from scattering of the carriers with underlying bosonic excitations. Below T_c the superconducting state displays a clear signature in the reflectance. However, the reflectance is a complex quantity consisting of an amplitude and a phase, $\tilde{r} = \sqrt{R} \exp(i\theta)$. Normally, only the amplitude $R = \tilde{r}\tilde{r}^*$ is measured so it is not always intuitively obvious what changes in the

reflectance indicate. For this reason, the complex optical properties have been calculated from a Kramers-Kronig analysis of the reflectance.⁷⁸

The temperature dependence of the real part of the optical conductivity $\sigma_1(\omega)$ of $\text{BaFe}_{1.85}\text{Co}_{0.15}\text{As}_2$ in the far-infrared region is shown in Fig. 3. At room temperature the conductivity decreases slowly with increasing frequency giving way, not unlike the high- T_c cuprates,⁷⁹ to a rather flat response in the mid-infrared region followed by a pronounced peak at about 5200 cm^{-1} (shown in the inset). At room temperature a weak infrared-active E_u mode at about 94 cm^{-1} is observed that involves in-plane displacements of the Ba atoms,⁴⁶ a second E_u mode expected at 253 cm^{-1} is a weak feature observed only at low temperatures, suggesting that this mode may be broadened due to disorder effects.⁸⁰ As the temperature is reduced the low-frequency conductivity increases as a result of the transfer of spectral weight from high to low frequencies, and the low-frequency E_u mode becomes more difficult to observe. The spectral weight is defined simply as the area under the conductivity curve over a given interval, $N(\omega, T) = \int_0^\omega \sigma_1(\omega', T) d\omega'$. It is important to note that the values for the dc conductivity in Fig. 1 at 295, 200 and 27 K are in good agreement with the extrapolated values $\sigma_{dc} \equiv \sigma_1(\omega \rightarrow 0)$ in Fig. 3; the fact that $\sigma_{dc} \approx \sigma_1(\omega \rightarrow 0)$ establishes a connection with transport and illustrates the self-consistent nature of this optical technique.

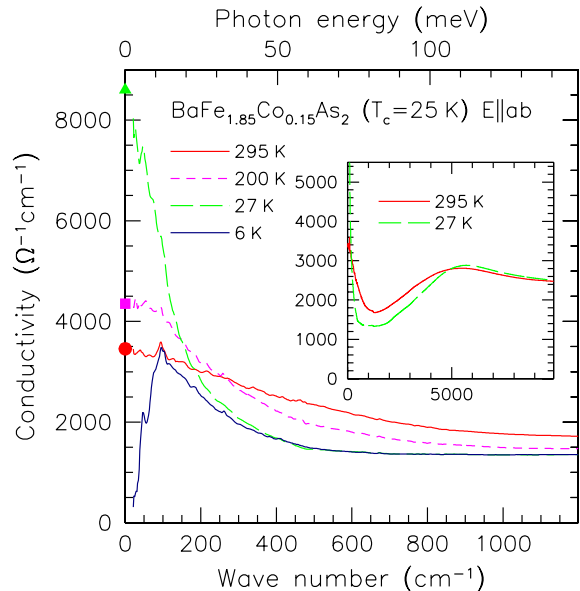


FIG. 3. The real part of the optical conductivity of $\text{BaFe}_{1.85}\text{Co}_{0.15}\text{As}_2$ in the infrared region for light polarized in the a - b planes at several temperatures above and below T_c . The extrapolated values for $\sigma_{dc} \equiv \sigma_1(\omega \rightarrow 0)$ agrees quite well with the dc transport data from Fig. 1 at 295 K (●), 200 K (■) and 27 K (▲). Below T_c there is a dramatic loss of low-frequency spectral weight due to the formation of a condensate. Inset: The conductivity at 295 and 27 K over a much wider frequency range.

TABLE I. The parameters for the Drude-Lorentz fits to in-plane optical conductivity at 27 K, where $1/\tau_{D,j}$ and $\omega_{p,D;j}$ are the scattering rate and plasma frequency for the j th Drude component (D_j), and ω_k , γ_k and Ω_k are the frequency, width and oscillator strength of the k th mode (L_k). The top frame is the result from considering two Drude and a single Lorentz oscillator. The second frame considers two Drude and two Lorentz components, while the bottom frame considers a single Drude component and two Lorentz oscillators. All units are in cm^{-1} , unless otherwise indicated.

Type	ω_k	$1/\tau_{D,j}, \gamma_k$	$\omega_{p,D;j}, \Omega_k$	l (\AA)
D ₁		113	6943	58
D ₂		5720	19980	0.4
L ₁	5170	5730	22070	
D ₁		126	7790	53
D ₂		608	1956	3.5
L ₁	1124	5560	18930	
L ₂	5190	5780	22470	
D ₁		126	7840	53
L ₁	1016	5070	18250	
L ₂	5200	5870	22980	

One technique to reproduce the optical conductivity assumes that because these materials are multiband systems that the free-carrier response can be described by separate contributions from the electron and hole pockets, while the optical properties at high frequency are described by bound excitations. In a Drude-Lorentz model, this description results in the linear combination of two Drude components.⁵⁹ The Drude-Lorentz model for the dielectric function $\tilde{\epsilon}(\omega) = \epsilon_1(\omega) + i\epsilon_2(\omega)$ can be written as

$$\tilde{\epsilon}(\omega) = \epsilon_\infty - \sum_j \frac{\omega_{p,D;j}^2}{\omega^2 + i\omega/\tau_{D,j}} + \sum_k \frac{\Omega_k^2}{\omega_k^2 - \omega^2 - i\omega\gamma_k},$$

where ϵ_∞ is the real part of the dielectric function at high frequency, $\omega_{p,D;j}^2 = 4\pi n_j e^2 / m_j^*$ and $1/\tau_{D,j}$ are the square of the plasma frequency and scattering rate for the delocalized (Drude) carriers in the j th pocket, respectively; ω_k , γ_k and Ω_k are the position, width, and strength of the k th vibration or excitation. The complex conductivity is $\tilde{\sigma}(\omega) = \sigma_1(\omega) + i\sigma_2(\omega) = -i\omega[\tilde{\epsilon}(\omega) - \epsilon_\infty]/4\pi$.

The results of the two-Drude fit to the real part of the optical conductivity just above T_c at 27 K are shown in Fig. 4(a) and summarized in Table I. The two Drude responses may be characterized as “narrow” ($1/\tau_D \simeq 113 \text{ cm}^{-1}$) and “broad” ($1/\tau_D \simeq 5700 \text{ cm}^{-1}$); an additional Lorentz oscillator at $\simeq 5200 \text{ cm}^{-1}$ has also been included as well as several others above 1 eV that are not allowed to vary (not listed in Table I). While the fit to the data is quite good, the scattering rate for the broad Drude component is more than 50 times that of the narrow component, which raises the issue as to whether this represents a mean-free path $l_j = v_{F,j}\tau_j$ that is physically meaningful ($v_{F,j}$ is the Fermi velocity and τ_j is the scattering time of the j th pocket). There are a range of values in the literature for the Fermi velocities for the electron

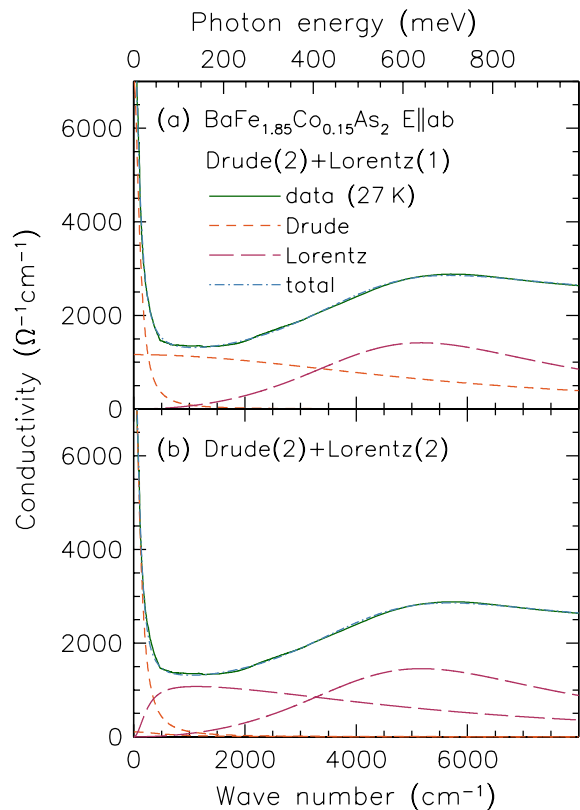


FIG. 4. (a) The two-Drude and single Lorentz oscillator fit to the data at 27 K over a wide frequency range. The Drude responses can be characterized by narrow and broad bands, with a single Lorentz oscillator centered at $\simeq 5200 \text{ cm}^{-1}$. (b) The fit to the data at 27 K using a two Drude components and two Lorentz oscillators. A significant portion of the spectral weight of the broad Drude component has been transferred to the low-frequency Lorentz oscillator. The results of the fits are summarized in Table I.

and hole pockets in the iron-arsenic materials. Based on photoemission study of BaFe_{1.85}Co_{0.15}As₂ (Ref. 43), we estimate that the Fermi velocity of the hole pocket to be $v_F \simeq 270 \text{ meV}\cdot\text{\AA}$, or $v_F \simeq 6.5 \times 10^5 \text{ cm/s}$. This result is less than the value determined from a band structure estimate of v_F for the hole pocket in a related material ($\simeq 8 \times 10^6 \text{ cm/s}$).⁶⁹ However, it has been noted that band-structure results often have to be renormalized to agree with photoemission results.⁸¹ The velocity of electron pocket is more difficult to calculate. As an estimate we will use the renormalization of the hole pocket Fermi velocity to the band structure estimate of v_F on the electron pocket⁶⁹ to obtain $v_F \simeq 2 \times 10^6 \text{ cm/s}$. We associate the narrower Drude component with the electron pocket with $\tau = 2.9 \times 10^{-13} \text{ s}$ which leads to a mean-free path of $l_e \simeq 58 \text{ \AA}$, or about 15 unit cells ($a \simeq 4 \text{ \AA}$ in the I4/mmm setting). Associating the broad Drude component with the hole pocket with $\tau \simeq 5.8 \times 10^{-15} \text{ s}$ leads to a mean-free path of $l_h \simeq 0.4 \text{ \AA}$, which is less than the shortest interatomic spacing; even a substantial increase in v_F will not alter this condition. This places the mean-free path

below the Mott-Ioffe-Regel limit^{82–84} and indicates that the conductivity in this band is no longer metallic but is instead incoherent, and is best described by a bound excitation, or a series of bound excitations.

This suggests that it is appropriate to include a low-frequency bound excitation which may arise from localization effects or from interband transitions.^{55,85} We have therefore considered the case of two Drude contributions as well as two low-frequency Lorentz oscillators; as in the previous case oscillators above 1 eV are not fitted quantities nor are their values changed from the previous instance. The results of the fit to the data at 27 K are shown in Fig. 4(b) and are summarized in the middle frame of Table I. The narrow Drude component at 27 K is only slightly broader than the same component in the previous approach, resulting in a slightly shorter mean-free path for the electron pocket $l_e \simeq 53$ Å. Much of the spectral weight formerly associated with the broad Drude component has shifted to a Lorentzian centered at $\simeq 1100$ cm⁻¹, resulting in a dramatic reduction of the scattering rate, $1/\tau \simeq 600$ cm⁻¹ and a commensurate increase of the mean-free path $l_h \simeq 3.5$ Å or $l_h \simeq a$; this value is still close to the Mott-Ioffe-Regel limit and it is debatable as to whether or not this constitutes metallic transport. While the uncertainties associated with most of the fitted parameters (determined from the covariance) are $\lesssim 5\%$, the broad and weak Drude component is difficult to fit and the errors associated with it are considerably larger, $\approx 20\%$. If there are indeed two Drude components then the electron pocket dominates and the hole pocket represents at best a weak, possibly incoherent, background contribution as shown in Fig. 4(b).

For completeness we have also considered the case of a single Drude component and two low-frequency Lorentz oscillators; the results of this fit are summarized at the bottom of Table I. With the exception of the absence of the second Drude component, the results are essentially the same as Fig. 4(b). The width of the narrow Drude component is unchanged and the slight increase in strength reflects the fact that it has absorbed the spectral weight formerly associated with the broad Drude component. We conclude that despite the presence of multiple bands in this material, for optimal doping the normal-state transport is dominated by the single electron pocket. The fitted values for the Drude parameters at 295, 200 and 27 K are $\omega_{p,D} = 7840$ cm⁻¹ (or 0.972 eV) and $1/\tau_D = 304, 233$ and 126 cm⁻¹, respectively.

2. Superconducting state

Below T_c there is a dramatic decrease in the low-frequency optical conductivity due to the formation of a superconducting energy gap. This “missing area” is referred to as the spectral weight of the condensate N_c and may be calculated from the Ferrell-Glover-Tinkham

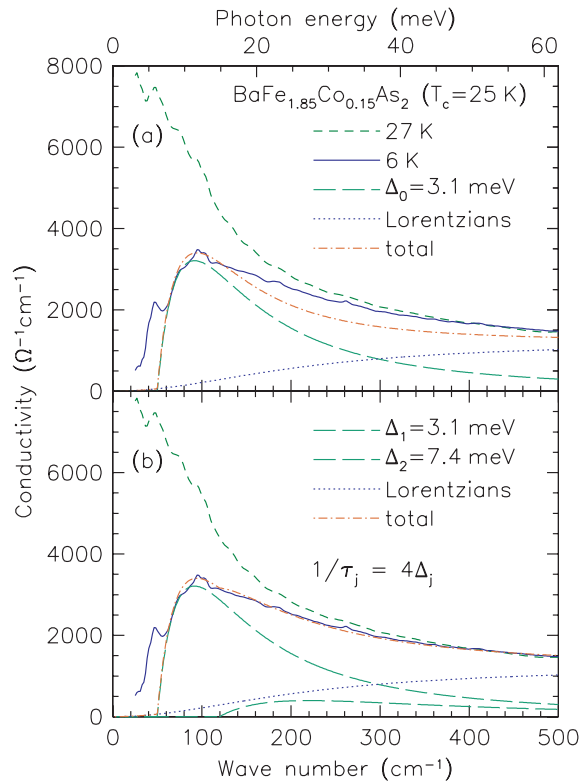


FIG. 5. The in-plane optical conductivity of the iron-arsenic superconductor $\text{BaFe}_{1.85}\text{Co}_{0.15}\text{As}_2$ ($T_c = 25$ K) shown at 27 and 6 K (dashed and solid lines, respectively). (a) The optical conductivity with a single isotropic s -wave gap of $\Delta_0 = 3.1$ meV with a scattering rate $1/\tau = 4\Delta_0$ is calculated for $T \ll T_c$ (long-dashed line) and superimposed on the contribution from the bound excitations in the mid-infrared (dotted line); the linear combination of the two curves (dot-dash line) does not reproduce the data well above ≈ 140 cm⁻¹. (b) The optical conductivity with isotropic s -wave gaps of $\Delta_1 = 3.1$ meV and $\Delta_2 = 7.4$ meV with the scattering rates $1/\tau_j = 4\Delta_j$ is calculated for $T \ll T_c$ and superimposed on the Lorentzian contribution; the linear combination of the three curves is in much better agreement with the measured data.

sum rule^{86,87}

$$N_c \equiv N(\omega_c, T \simeq T_c) - N(\omega_c, T \ll T_c) = \omega_{p,S}^2/8.$$

Here $\omega_{p,S}^2 = 4\pi n_s e^2/m^*$ is the square of the superconducting plasma frequency and superfluid density is $\rho_{s0} \equiv \omega_{p,S}^2$; the cut-off frequency $\omega_c \simeq 400$ cm⁻¹ is chosen so that the integral converges smoothly. The superconducting plasma frequency has also been determined from $\epsilon_1(\omega)$ in the low frequency limit where $\epsilon_1(\omega) = \epsilon_\infty - \omega_{p,S}^2/\omega^2$. Yet another method of extracting $\omega_{p,S}$ from $\epsilon_1(\omega)$ is to determine $[-\omega^2\epsilon_1(\omega)]^{1/2}$ in the $\omega \rightarrow 0$ limit.⁸⁸ All three techniques yield $\omega_{p,S} \simeq 5200 \pm 400$ cm⁻¹, indicating that less than one-half of the free-carriers in the normal state have condensed ($\omega_{p,S}^2/\omega_{p,D}^2 \lesssim 0.5$). In a clean-limit system the scattering rate associated with the Drude free-carrier response is much smaller than the size of the fully-formed isotropic superconduct-

ing energy gap $1/\tau \ll 2\Delta_0$. As a result the full spectral weight of the Drude component lies below the optical gap $2\Delta_0$; for $T \ll T_c$ all of the free carriers collapse into the condensate and $\omega_{p,S} \equiv \omega_{p,D}$. In materials where the size of the free-carrier scattering rate and the optical gap are comparable, $1/\tau \gtrsim 2\Delta_0$ (the so-called dirty limit) a significant amount of the Drude spectral weight lies above $2\Delta_0$. As a result for $T \ll T_c$ the free carriers are gapped and there is no residual Drude component at low temperature; however, only a fraction of the Drude spectral weight below the optical gap $2\Delta_0$ collapses into the condensate, leading to the condition that $\omega_{p,S} < \omega_{p,D}$. This is precisely what we observe, implying that this material is not in the clean limit. The superfluid density can also be expressed as an effective penetration depth $\lambda_0 \simeq 3000 \pm 300 \text{ \AA}$, which is in good agreement with other optical measurements^{55–60} as well as estimates based on other techniques for materials with similar cobalt concentrations.^{89–91}

The low-frequency optical conductivity is shown in more detail in Fig. 5. As previously noted, below T_c there is a dramatic reduction of the conductivity below about 80 cm^{-1} ($\approx 10 \text{ meV}$), which sets the energy scale for the superconducting energy gap Δ_0 and the optical gap $2\Delta_0$ [here we adopt the convention that $\Delta_j \equiv \Delta_j(0)$]. We note that based on this initial estimate it appears that $1/\tau_D \gtrsim 2\Delta_0$, suggesting that the conductivity in this material can be modeled using a Mattis-Bardeen approach⁹² for the contribution from the gapped excitations.⁹³ This dirty-limit approach is consistent with the observation that less than 50% of the free carriers in the normal state collapse into the condensate for $T \ll T_c$. Note that in this instance, “dirty” refers to scattering from disorder and/or electronic correlations in addition to any possible impurity effects. In Fig. 5(a) the optical conductivity in the superconducting state is described by a single isotropic gap $\Delta_0 \simeq 3.1 \text{ meV}$ ($T \ll T_c$) with a moderate amount of elastic scattering [$1/\tau = 4\Delta_0$, which is approximately the previously determined value of $1/\tau_D$ just above T_c] in linear combination with the low-frequency tails of the mid-infrared Lorentzian oscillators. While the leading-edge of the conductivity is described fairly well, there is a noticeable disagreement above about 140 cm^{-1} .

To properly model the conductivity over the entire far-infrared region, two isotropic gap features are considered at $\Delta_1 = 3.1 \text{ meV}$ and $\Delta_2 = 7.4 \text{ meV}$ with $1/\tau_j = 4\Delta_j$ for $T \ll T_c$. In combination with the Lorentzian tails, the two-gap scenario shown in Fig. 5(b) fits the data quite well. The gap amplitudes determined here are in excellent agreement with recent optical results on $\text{BaFe}_{2-x}\text{Co}_x\text{As}_2$ for a similar cobalt concentration,^{54,55} as well as photoemission⁴² and tunneling results.⁹⁴ While the lower gap ratio $2\Delta_1/k_B T_c \simeq 2.9$ is close to the BCS weak coupling limit of 3.5, the upper gap ratio $2\Delta_2/k_B T_c \simeq 7.3$ is considerably larger. While the data below about 40 cm^{-1} is not reproduced exactly, there is a considerable uncertainty associated with the conductivity in this spectral region. This suggestion that the Fermi

surface is completely gapped in the optimally-doped material is in agreement with thermodynamic studies.^{34,35}

The examination of the normal-state concluded that while the low-frequency optical properties were dominated by the electron pocket, a weak contribution from the hole pocket might also be present. In the formalism employed here, the inclusion of a second gap necessarily implies a second band. The calculated Drude response just above T_c in Fig. 5(b) for the two bands (not shown) is $\sigma_{1,j}(\omega) = \sigma_{0,j}/(1 + \omega^2\tau_j^2)$, where $\sigma_{0,1} \approx 7700 \text{ \Omega}^{-1}\text{cm}^{-1}$ and $\sigma_{0,2} \approx 850 \text{ \Omega}^{-1}\text{cm}^{-1}$ for the bands associated with the small and large gaps, respectively. Given that $\sigma_{0,j} = \omega_{p,D;j}^2\tau_j/60$, where $\omega_{p,D;j}$ is the plasma frequency associated with the j th band, and $\omega_{p,D} \simeq (\omega_{p,D;1}^2 + \omega_{p,D;2}^2)^{1/2}$ and recalling that $\tau_j = 4\Delta_j$, we estimate that $\omega_{p,D;1} \simeq 6800 \text{ cm}^{-1}$ and $\omega_{p,D;2} \simeq 3500 \text{ cm}^{-1}$. Once again it is the case that a single band dominates and that over 75% of the superconducting condensate originates from the gapping of this band.

In the simple approach employed here, the two energy scales for the gaps result from the gapping of two separate bands. This view is consistent with ARPES measurements^{36,38–42} that indicate that both the electron and hole pockets are likely completely gapped below T_c . However, it is clear that the coherent transport in the normal state arises mainly from the electron pocket. It is therefore also possible that the two energy scales for the superconducting energy gaps observed here are due to single anisotropic s -wave gap on the electron pocket, which is favored within the s^\pm model. Because there is some uncertainty in the optical measurements with respect to the amplitude of the larger gap, time-domain measurements were performed.

B. Time-domain spectroscopy

The details of the superconducting gap properties have been investigated in the time-domain. Fig. 6(a) shows the time evolution of the photo-induced reflectivity change, $\Delta R/R$ as a function of temperature at 800 nm. The data is fitted by $\Delta R/R = A_0 + A_{fast} \exp(-t/\tau_{fast}) + A_{slow} \exp(-t/\tau_{slow})$; $\Delta R/R$ shows a bi-exponential decay with relaxation times $\tau_{fast} \simeq 0.2 \text{ ps}$ and $\tau_{slow} \simeq 15 \text{ ps}$. These two decay signals are the result of Cooper-pair recombination following the photo-excitation. Figs. 6(b) and 6(c) show the temperature dependence of the relaxation times (τ_{fast} and τ_{slow}) and the peak amplitudes are shown in the insets (A_{fast} and A_{slow}). The fact that $\Delta R/R$ does not return to its value at $t < 0$ above about 45 ps is due to a negative component with a long relaxation time ($\sim \text{ns}$), not a rise time. This negative component is a common feature in photo-induced reflectivity measurements of complex metallic systems involving magnetism such as colossal magnetoresistance materials⁹⁵ and the high- T_c cuprates;⁹⁶ this component is not related to the superconductivity. The phenomenological Rothwarf-Taylor (RT) model⁹⁷ is used to

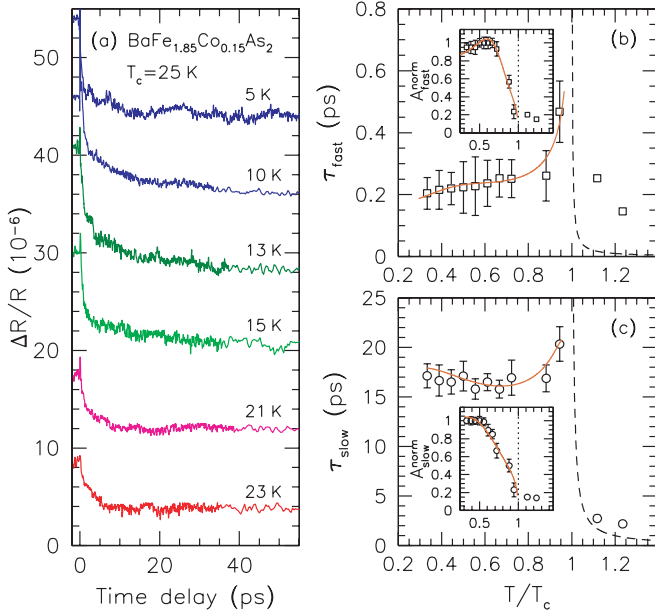


FIG. 6. (a) The time evolution of the photo induced reflectivity change, $\Delta R/R$ in $\text{BaFe}_{1.85}\text{Co}_{0.15}\text{As}_2$ as a function of temperature (below T_c) at 800 nm (the spectra are offset for clarity). (b) Temperature dependence of the relaxation time, τ_{fast} . The inset shows the normalized amplitude A_{fast} . Solid lines are fits to the RT model, yielding $\Delta_2 \approx 7.4 \pm 1.2$ meV; (c) Temperature dependence of the relaxation time, τ_{slow} . The inset shows the normalized amplitude A_{slow} . Solid lines are fits to the RT model, yielding $\Delta_1 \approx 3.5 \pm 0.4$ meV.

describe the quasiparticle dynamics

$$\frac{dn}{dt} = I_0 + \beta N - Rn^2$$

and

$$\frac{dN}{dt} = -\frac{\beta N}{2} + \frac{Rn^2}{2} - (N - N_T)\gamma.$$

Here n and N are the total density of quasiparticles and high-frequency bosons, respectively, β is the probability for pair breaking by high-frequency boson absorption, R is the bare quasiparticle recombination rate, N_T is the density of high-frequency bosons in equilibrium, and γ is their decay rate. We obtain the normalized amplitude of the signal (to its low-temperature value), $A(T)$ via the relation: $A(T) \propto (n_T - 1)^{-1}$, where the density of the thermally excited quasiparticles, $n_T \propto \sqrt{\Delta(T)T} \exp[-\Delta(T)/T]$, with $\Delta(0)$ as a fitting parameter and $\Delta(T)$ obeying a BCS temperature dependence. Moreover, for a constant pump intensity and assuming γ is temperature independent, we obtain the temperature dependence of the relaxation time τ by the temperature dependence of n_T :

$$\tau(T)^{-1} = \Gamma \left[A(T) + b\sqrt{\Delta(T)T} \exp(-\Delta(T)/T) \right],$$

where Γ and B are fitting parameters. Since the temperature dependence of $A(T)$ and $\tau(T)$ are measured

directly, we can accurately determine the values of the superconducting gaps, $\Delta_1 = 3.5 \pm 0.4$ meV and $\Delta_2 = 7.4 \pm 1.2$ meV. These gap values are in excellent agreement with the optical estimates determined in the previous section.

C. Electron-phonon coupling

The temperature dependence of the *ab*-plane resistivity (Fig. 1) has been fit using the generalized Bloch-Grüneisen formula^{98–101}

$$\rho(T) = \rho_0 + \lambda_{ph}(m-1) \left(\frac{k_B \Theta_D}{\omega_{p,D}^2} \right) \left(\frac{T}{\Theta_D} \right)^m J_m \left(\frac{T}{\Theta_D} \right)$$

where

$$J_m \left(\frac{T}{\Theta_D} \right) = \int_0^{\Theta_D/T} \frac{x^m e^{-x}}{(1 - e^{-x})^2} dx.$$

In this instance the integer value $m = 5$ implies that the resistance is due to the scattering of electrons by phonons. The Debye temperature Θ_D is set to 250 K (Ref. 102), and the plasma frequency has been previously determined to be $\omega_{p,D} = 0.972 \pm 0.05$ eV. The fit, shown by the dashed curve in Fig. 1 yields $\rho_0 \approx 125$ m Ω -cm and an upper bound for the transport electron-phonon coupling constant $\lambda_{ph} \approx 0.2 \pm 0.02$. This experimental estimate of λ_{ph} value is in excellent agreement with the theoretical value of $\lambda \approx 0.21$ (Ref. 14) which yields a maximum $T_c \approx 0.8$ K. However, to get a more accurate estimate of the electron-boson coupling constant from the resistivity, the temperature dependence of the underlying bosonic spectra needs to be considered.

D. Electron-boson coupling

The kinks observed in the normal-state reflectance in Fig. 2 at ≈ 12 and 55 meV suggest scattering from underlying bosonic excitations. In order to investigate this further the generalized Drude model has been considered in which the scattering rate and the effective mass are allowed to adopt a frequency dependence^{103,104}

$$\frac{1}{\tau(\omega)} = \frac{\omega_p^2}{4\pi} \text{Re} \left[\frac{1}{\tilde{\sigma}(\omega)} \right]$$

and

$$\frac{m^*(\omega)}{m_b} = \frac{\omega_p^2}{4\pi\omega} \text{Im} \left[\frac{1}{\tilde{\sigma}(\omega)} \right],$$

where the m_b is the bandmass; $m^*(\omega)/m_b = 1 + \lambda(\omega)$ and $\lambda(\omega)$ is a frequency-dependent electron-boson coupling constant. In this instance we set $\omega_p \equiv \omega_{p,D}$ and $\epsilon_\infty = 4$ (although the choice of ϵ_∞ has little effect on the

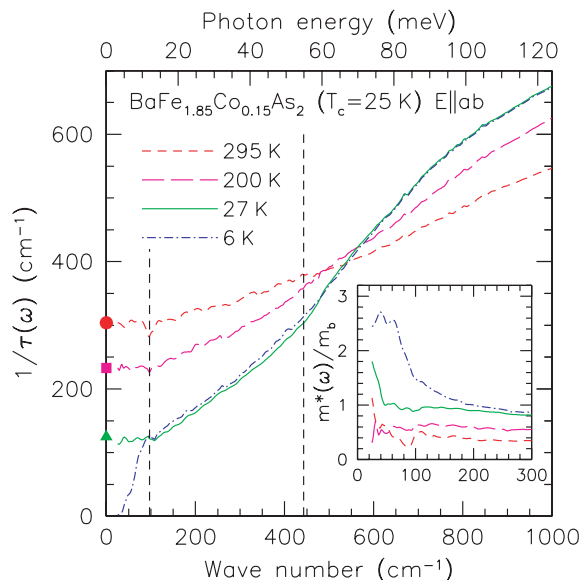


FIG. 7. The in-plane frequency-dependent scattering rate of $\text{BaFe}_{1.85}\text{Co}_{0.15}\text{As}_2$ for several temperatures above and below T_c in the far-infrared region. The values for $1/\tau_D$ are shown at 295 (●), 200 (■) and 27 K (▲), respectively, where the scattering rate displays little temperature dependence. The dashed lines at $\simeq 12$ and 55 meV indicate changes in the slope of $1/\tau(\omega)$. Inset: The frequency dependence of the effective mass.

scattering rate or the effective mass in the far-infrared region). The temperature dependence of $1/\tau(\omega)$ is shown in Fig. 7, and the inset shows the temperature dependence of $m^*(\omega)/m_b$. In the normal state, in accord with the Drude model, the scattering rate is constant below $\simeq 100$ cm^{-1} and $1/\tau(\omega \rightarrow 0) \simeq 1/\tau_D$. However, above $\simeq 12$ meV there is an abrupt increase in the scattering rate for [the large change in $1/\tau(\omega)$ for $T \ll T_c$ is due to the formation of one or more superconducting energy gaps]; another kink is observed at $\simeq 55$ meV. Interestingly, the effective mass enhancement is rather small $m^*(\omega \rightarrow 0)/m_b \simeq 2$, indicating that the electron-boson coupling $\lambda \equiv \lambda(\omega \rightarrow 0) \simeq 1$; this is significantly smaller than the values of $\lambda \simeq 3 - 4$ that have recently been reported.^{52,105}

The electron-boson spectral function can in be calculated from $1/\tau(\omega)$ using a maximum-entropy technique based on Eliashberg theory.¹⁰⁶ Such an analysis has recently been performed on a material with an almost identical cobalt concentration and will not be repeated here; the peaks in the electron-boson spectral function in that work¹⁰⁵ are observed at $\simeq 10$ and 45 meV, which is in good agreement with the kinks observed in the present study in $1/\tau(\omega)$ at $\simeq 12$ and 55 meV. The low-energy peak is associated with the resonance peak in the spin excitation spectrum obtained from inelastic neutron scattering data,¹⁰⁷ which when considered with the relatively weak electron-phonon interaction in this material, suggests that the superconductivity in this material may be

mediated by magnetic interactions.¹⁰⁵ The high-energy kink lies above the highest measured phonon energy;¹⁰⁸ however, muon-spin relaxation measurements¹⁰⁹ on a number of iron pnictides suggest an antiferromagnetic energy scale of $\simeq 50$ meV indicating a possible magnetic origin for this feature. It is not clear if this boson plays a role in the superconductivity or not; however, we speculate that any mechanism that did couple to the high-energy boson might display a significantly enhanced T_c , suggesting that higher values for T_c in this class of materials may yet be possible.

E. Scaling of the superfluid density

It has been demonstrated that a Uemura-type of scaling between the superfluid density ρ_{s0} and T_c breaks down in the hole-doped $\text{Ba}_{0.6}\text{K}_{0.4}\text{Fe}_2\text{As}_2$ material.²⁴ However, it has also been demonstrated that a number of the iron pnictide and chalcogenide materials^{110,111} the superfluid density falls on a recently proposed empirical scaling relation for the cuprate superconductors,^{112,113} shown by the dashed line in Fig. 8,

$$\rho_{s0}/8 \simeq 4.4 \sigma_{dc} T_c.$$

From the estimate of $\sigma_{dc} \equiv \sigma_1(\omega \rightarrow 0) \simeq 8000 \pm 400 \Omega^{-1}\text{cm}^{-1}$ for $T \gtrsim T_c$ (determined from Fig. 3, as well as Drude-Lorentz fits), and the previously determined value of $\rho_{s0} = 27 \pm 3 \times 10^6 \text{ cm}^{-2}$, we can see that $\text{BaFe}_{1.85}\text{Co}_{0.15}\text{As}_2$ also falls on this scaling line in the region of the moderately-underdoped cuprates. The dotted

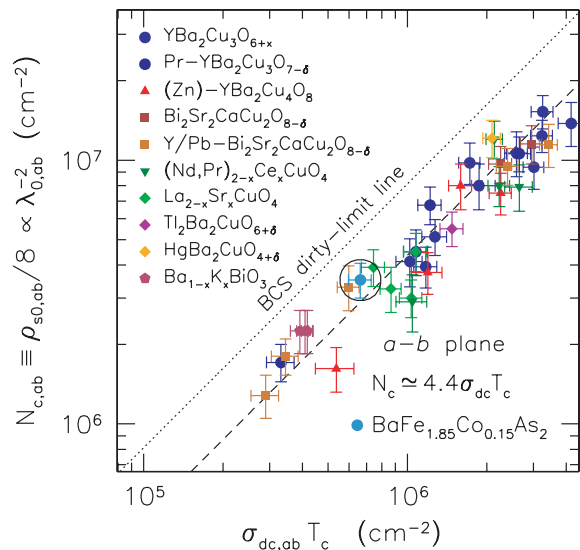


FIG. 8. The log-log plot of the in-plane spectral weight of the superfluid density $N_c \equiv \rho_{s0}/8$ vs $\sigma_{dc} T_c$, for a variety of electron and hole-doped cuprates compared with the result for $\text{BaFe}_{1.85}\text{Co}_{0.15}\text{As}_2$. The dashed line corresponds to the general result for the cuprates $\rho_{s0}/8 \simeq 4.4 \sigma_{dc} T_c$, while the dotted line is the result expected for a BCS dirty-limit superconductor in the weak-coupling limit, $\rho_{s0}/8 \simeq 8.1 \sigma_{dc} T_c$.

line in Fig. 8 is the calculated result for a BCS dirty-limit superconductor in the weak-coupling limit in which the numerical constant in the scaling relation is calculated to be slightly larger,¹¹³ $\rho_{s0}/8 \simeq 8.1\sigma_{dc}T_c$. This scaling behavior is consistent with the observation that this material is not in the clean limit.

IV. CONCLUSIONS

The optical and transport properties of the iron-arsenic superconductor $\text{BaFe}_{1.85}\text{Co}_{0.15}\text{As}_2$ ($T_c = 25$ K) have been measured over a wide temperature and frequency range. A Bloch-Grüneisen analysis of the resistivity indicates that the electron-phonon coupling $\lambda_{ph} \simeq 0.2$ is fairly weak, suggesting that the superconductivity in this material is not mediated by lattice vibrations. The optical properties in the normal state are dominated by the electron pocket and may be described as a weakly-interacting Fermi liquid, or Drude model, with $\omega_{p,D} \simeq 7840 \text{ cm}^{-1}$ and $1/\tau_D \simeq 126 \text{ cm}^{-1}$ just above T_c at 27 K. The frequency-dependent scattering rate displays kinks at $\simeq 12$ and 55 meV that correspond to peaks in the electron-boson spectral function, both of which are believed to be magnetic in origin, and suggest that the pairing in this material may be mediated by magnetic interactions. In the superconducting state for $T \ll T_c$ the superconducting plasma frequency $\omega_{p,S} \simeq 5200 \text{ cm}^{-1}$, which corresponds to an effective penetration depth of

$\lambda \simeq 3000 \text{ \AA}$. This indicates that only about 50% of the free-carriers in the normal-state condense into the condensate, suggesting this material is not in the clean limit. In agreement with the results of other workers, this material is observed to fall on the universal scaling line for a BCS dirty-limit superconductor, and is also close to many underdoped cuprates. The energy scales observed for the superconducting energy gaps $\Delta_1 \simeq 3.1$ meV and $\Delta_2 \simeq 7.4$ meV correspond to either the gaps on the electron and hole pockets, respectively, or the minimum and maximum values for an anisotropic s -wave gap on the electron pocket, in accord with the s^\pm model. The spectrum of excitations appears to be fully gapped, suggesting an absence of nodes at optimal doping in this material.

ACKNOWLEDGMENTS

We would like to thank A. Akrap, J. L. Birman, G. L. Carr, A. V. Chubukov, K. Felix, D. H. Lee, I. Mazin, P. Richard, E. Schachinger, D. J. Singh and H. Yang and for helpful discussions, and J. P. Carbotte for performing an inversion of the optical data. Work was supported by the National Science Foundation, and the National Science Foundation of China. Work at Brookhaven National Laboratory was supported in part by the Office of Science, U.S. Department of Energy under Contract No. DE-AC02-98CH10886.

* homes@bnl.gov

¹ J. Bardeen, L. N. Cooper, and J. R. Schrieffer, *Phys. Rev.* **108**, 1175 (1957).
² W. L. McMillan, *Phys. Rev.* **167**, 331 (1968).
³ J. G. Bednorz and K. A. Mueller, *Z. Phys. B* **64**, 189 (1986).
⁴ D. J. Van Harlingen, *Rev. Mod. Phys.* **67**, 515 (1995).
⁵ J. Nagamatsu, N. Nakagawa, T. Muranaka, Y. Zenitani, and J. Akimitsu, *Nature (London)* **410**, 63 (2001).
⁶ S. L. Bud'ko, G. Lapertot, C. Petrovic, C. E. Cunningham, N. Anderson, and P. C. Canfield, *Phys. Rev. Lett.* **86**, 1877 (2001).
⁷ J. Kortus, I. I. Mazin, K. D. Belashchenko, V. P. Antropov, and L. L. Boyer, *Phys. Rev. Lett.* **86**, 4656 (2001).
⁸ Y. Kamihara, T. Watanabe, M. Hirano, and H. Hosono, *J. Am. Chem. Soc.* **130**, 3296 (2008).
⁹ Z.-A. Ren, J. Yang, W. Lu, W. Yi, X.-L. Shen, Z.-C. Li, G.-C. Che, X.-L. Dong, L.-L. Sun, F. Zhou, and Z.-X. Zhao, *EPL* **82**, 57002 (2008).
¹⁰ Z.-A. Ren, G.-C. Che, X.-L. Dong, J. Yang, W. Lu, W. Yi, X.-L. Shen, Z.-C. Li, L.-L. Sun, F. Zhou, and Z.-X. Zhao, *EPL* **83**, 17002 (2008).
¹¹ C. Wang, L. Li, S. Chi, Z. Zhu, Z. Ren, Y. Li, Y. Wang, X. Lin, Y. Luo, S. Jiang, X. Xu, G. Cao, and Z. Xu, *EPL* **83**, 67006 (2008).

¹² K. Ishida, Y. Nakai, and H. Hosono, *J. Phys. Soc. Japan* **78**, 062001 (2009).
¹³ C. de la Cruz, Q. Huang, J. W. Lynn, J. Li, W. Ratcliff II, J. L. Zarestky, H. A. Mook, G. F. Chen, J. L. Luo, N. L. Wang, and P. Dai, *Nature (London)* **453**, 899 (2008).
¹⁴ L. Boeri, O. V. Dolgov, and A. A. Golubov, *Phys. Rev. Lett.* **101**, 026403 (2008).
¹⁵ L. Boeri, O. Dolgov, and A. Golubov, *Physica C* **469**, 628 (2009).
¹⁶ I. I. Mazin, *Nature* **464**, 183 (2010).
¹⁷ D. C. Johnston, *Adv. Phys.* **59**, 803 (2010).
¹⁸ M. Rotter, M. Tegel, D. Johrendt, I. Schellenberg, W. Hermes, and R. Pöttgen, *Phys. Rev. B* **78**, 020503 (2008).
¹⁹ P. L. Alireza, Y. T. C. Ko, J. Gillett, C. M. Petrone, J. M. Cole, G. G. Lonzarich, and S. E. Sebastian, *J. Phys.: Condens. Matter* **21**, 012208 (2009).
²⁰ Z. Ren, Q. Tao, S. Jiang, C. Feng, C. Wang, J. Dai, G. Cao, and Z. Xu, *Phys. Rev. Lett.* **102**, 137002 (2009).
²¹ M. Rotter, M. Tegel, and D. Johrendt, *Phys. Rev. Lett.* **101**, 107006 (2008).
²² A. S. Sefat, R. Jin, M. A. McGuire, B. C. Sales, D. J. Singh, and D. Mandrus, *Phys. Rev. Lett.* **101**, 117004 (2008).
²³ L. J. Li, Q. B. Wang, Y. K. Luo, H. Chen, Q. Tao, Y. K. Li, X. Lin, M. He, Z. W. Zhu, G. H. Cao, and Z. A. Xu, *New J. Phys.* **11**, 025008 (2009).

- ²⁴ C. Ren, Z.-S. Wang, H.-Q. Luo, H. Yang, L. Shan, and H.-H. Wen, *Phys. Rev. Lett.* **101**, 257006 (2008).
- ²⁵ L. Fang, H. Luo, P. Cheng, Z. Wang, Y. Jia, G. Mu, B. Shen, I. I. Mazin, L. Shan, C. Ren, and H.-H. Wen, *Phys. Rev. B* **80**, 140508(R) (2009).
- ²⁶ J. T. Park, D. S. Inosov, C. Niedermayer, G. L. Sun, D. Haug, N. B. Christensen, R. Dinnebier, A. V. Boris, A. J. Drew, L. Schulz, T. Shapoval, U. Wolff, V. Neu, X. Yang, C. T. Lin, B. Keimer, and V. Hinkov, *Phys. Rev. Lett.* **102**, 117006 (2009).
- ²⁷ H. Q. Yuan, J. Singleton, F. F. Balakirev, S. A. Baily, G. F. Chen, J. L. Luo, and N. L. Wang, *Nature (London)* **457**, 565 (2009).
- ²⁸ C. Martin, R. T. Gordon, M. A. Tanatar, H. Kim, N. Ni, S. L. Bud'ko, P. C. Canfield, H. Luo, H. H. Wen, Z. Wang, A. B. Vorontsov, V. G. Kogan, and R. Prozorov, *Phys. Rev. B* **80**, 020501(R) (2009).
- ²⁹ S. L. Bud'ko, N. Ni, and P. C. Canfield, *Phys. Rev. B* **79**, 220516(R) (2009).
- ³⁰ F. Rullier-Albenque, D. Colson, A. Forget, and H. Alloul, *Phys. Rev. Lett.* **103**, 057001 (2009).
- ³¹ M. Yashima, H. Nishimura, H. Mukuda, Y. Kitaoka, K. Miyazawa, P. M. Shirage, K. Kihou, H. Kito, H. Eisaki, and A. Iyo, *Journal of the Physical Society of Japan* **78**, 103702 (2009).
- ³² K. Gofryk, A. S. Sefat, M. A. McGuire, B. C. Sales, D. Mandrus, J. D. Thompson, E. D. Bauer, and F. Ronning, *Phys. Rev. B* **81**, 184518 (2010).
- ³³ F. L. Ning, K. Ahilan, T. Imai, A. S. Sefat, M. A. McGuire, B. C. Sales, D. Mandrus, P. Cheng, B. Shen, and H.-H. Wen, *Phys. Rev. Lett.* **104**, 037001 (2010).
- ³⁴ M. A. Tanatar, J.-P. Reid, H. Shakeripour, X. G. Luo, N. Doiron-Leyraud, N. Ni, S. L. Bud'ko, P. C. Canfield, R. Prozorov, and L. Taillefer, *Phys. Rev. Lett.* **104**, 067002 (2010).
- ³⁵ J.-P. Reid, M. A. Tanatar, X. G. Luo, H. Shakeripour, N. Doiron-Leyraud, N. Ni, S. L. Bud'ko, P. C. Canfield, R. Prozorov, and L. Taillefer, *Phys. Rev. B* **82**, 064501 (2010).
- ³⁶ H. Ding, P. Richard, N. Nakayama, K. Sugawara, T. Arakane, Y. Sekiba, A. Takayama, S. Souma, T. Sato, T. Takahashi, Z. Wang, X. Dai, Z. Fang, G. F. Chen, J. L. Lou, and N. L. Wang, *EPL* **83**, 47001 (2008).
- ³⁷ C. Liu, G. D. Samolyuk, Y. Lee, N. Ni, T. Kondo, A. F. Santander-Syro, S. L. Bud'ko, J. L. McChesney, E. Rotenberg, T. Valla, A. V. Fedorov, P. C. Canfield, B. N. Harmon, and A. Kaminski, *Phys. Rev. Lett.* **101**, 177005 (2008).
- ³⁸ R. Khasanov, D. V. Evtushinsky, A. Amato, H.-H. Klauss, H. Luetkens, C. Niedermayer, B. Büchner, G. L. Sun, C. T. Lin, J. T. Park, D. S. Inosov, and V. Hinkov, *Phys. Rev. Lett.* **102**, 187005 (2009).
- ³⁹ D. V. Evtushinsky, D. S. Inosov, V. B. Zabolotnyy, A. Koitzsch, M. Knupfer, B. Büchner, M. S. Viazovska, G. L. Sun, V. Hinkov, A. V. Boris, C. T. Lin, B. Keimer, A. Varykhalov, A. A. Kordyuk, and S. V. Borisenko, *Phys. Rev. B* **79**, 054517 (2009).
- ⁴⁰ A. Koitzsch, D. S. Inosov, D. V. Evtushinsky, V. B. Zabolotnyy, A. A. Kordyuk, A. Kondrat, C. Hess, M. Knupfer, B. Büchner, G. L. Sun, V. Hinkov, C. T. Lin, A. Varykhalov, and S. V. Borisenko, *Phys. Rev. Lett.* **102**, 167001 (2009).
- ⁴¹ V. B. Zabolotnyy, D. S. Inosov, D. V. Evtushinsky, A. Koitzsch, A. A. Kordyuk, G. L. Sun, J. T. Park, D. Haug, V. Hinkov, A. V. Boris, C. T. Lin, M. Knupfer, A. N. Yaresko, B. Büchner, A. Varykhalov, R. Follath, and S. V. Borisenko, *Nature (London)* **457**, 569 (2009).
- ⁴² K. Terashima, Y. Sekiba, J. H. Bowen, K. Nakayama, T. Kawahara, T. Sato, P. Richard, Y.-M. Xu, L. J. Li, G. H. Cao, Z.-A. Xu, H. Ding, and T. Takahashi, *PNAS* **106**, 7330 (2009).
- ⁴³ Y. Sekiba, T. Sato, K. Nakayama, K. Terashima, P. Richard, J. H. Bowen, H. Ding, Y.-M. Xu, L. J. Li, G. H. Cao, Z.-A. Xu, and T. Takahashi, *New. J. Phys* **11**, 025020 (2009).
- ⁴⁴ C. Liu, T. Kondo, R. M. Fernandes, A. D. Palczewski, E. D. Mun, N. Ni, A. N. Thaler, A. Bostwick, E. Rotenberg, J. Schmalian, S. L. Budko, P. C. Canfield, and A. Kaminski, *Nature Phys.* **6**, 419 (2010).
- ⁴⁵ K. Nakayama, T. Sato, P. Richard, Y.-M. Xu, T. Kawahara, K. Umezawa, T. Qian, M. Neupane, G. F. C. and H. Ding, and T. Takahashi, arXiv:1009.4236 (unpublished).
- ⁴⁶ A. P. Litvinchuk, V. G. Hadjiev, M. N. Iliev, B. Lv, A. M. Guloy, and C. W. Chu, *Phys. Rev. B* **78**, 060503(R) (2008).
- ⁴⁷ L. Chauvière, Y. Gallais, M. Cazayous, A. Sacuto, M. A. Méasson, D. Colson, and A. Forget, *Phys. Rev. B* **80**, 094504 (2009).
- ⁴⁸ M. Rahlenbeck, G. L. Sun, D. L. Sun, C. T. Lin, B. Keimer, and C. Ulrich, *Phys. Rev. B* **80**, 064509 (2009).
- ⁴⁹ B. Muschler, W. Prestel, R. Hackl, T. P. Devereaux, J. G. Analytis, J.-H. Chu, and I. R. Fisher, *Phys. Rev. B* **80**, 180510(R) (2009).
- ⁵⁰ G. Li, W. Z. Hu, J. Dong, Z. Li, P. Zheng, G. F. Chen, J. L. Luo, and N. L. Wang, *Phys. Rev. Lett.* **101**, 107004 (2008).
- ⁵¹ W. Hu, Q. Zhang, and N. Wang, *Physica C* **469**, 545 (2009).
- ⁵² J. Yang, D. Hüvonen, U. Nagel, T. Rööm, N. Ni, P. C. Canfield, S. L. Bud'ko, J. P. Carbotte, and T. Timusk, *Phys. Rev. Lett.* **102**, 187003 (2009).
- ⁵³ D. Wu, N. Barišić, N. Drichko, S. Kaiser, A. Faridian, M. Dressel, S. Jiang, Z. Ren, L. J. Li, G. H. Cao, Z. A. Xu, H. S. Jeevan, and P. Gegenwart, *Phys. Rev. B* **79**, 155103 (2009).
- ⁵⁴ T. Fischer, A. V. Pronin, J. Wosnitza, K. Iida, F. Kurth, S. Haindl, L. Schultz, B. Holzapfel, and E. Schachinger, arXiv:1005.0692 (unpublished).
- ⁵⁵ E. van Heumen, Y. Huang, S. de Jong, A. B. Kuzmenko, M. S. Golden, and D. van der Marel, *EPL* **90**, 37005 (2010).
- ⁵⁶ K. W. Kim, M. Rössle, A. Dubroka, V. K. Malik, T. Wolf, and C. Bernhard, *Phys. Rev. B* **81**, 214508 (2010).
- ⁵⁷ B. Gorshunov, D. Wu, A. A. Voronkov, P. Kallina, K. Iida, S. Haindl, F. Kurth, L. Schultz, B. Holzapfel, and M. Dressel, *Phys. Rev. B* **81**, 060509(R) (2010).
- ⁵⁸ M. Nakajima, S. Ishida, K. Kihou, Y. Tomioka, T. Ito, Y. Yoshida, C. H. Lee, H. Kito, A. Iyo, H. Eisaki, K. M. Kojima, and S. Uchida, *Phys. Rev. B* **81**, 104528 (2010).
- ⁵⁹ D. Wu, N. Barišić, P. Kallina, A. Faridian, B. Gorshunov, N. Drichko, L. J. Li, X. Lin, G. H. Cao, Z. A. Xu, N. L. Wang, and M. Dressel, *Phys. Rev. B* **81**, 100512(R) (2010).
- ⁶⁰ P. Marsik, K. W. Kim, A. Dubroka, M. Rössle, V. K. Malik, L. Schulz, C. N. Wang, C. Niedermayer, A. J. Drew, M. Willis, T. Wolf, and C. Bernhard, *Phys. Rev. Lett.* **105**, 057001 (2010).

- ⁶¹ A. Perucchi, L. Baldassarre, C. Marini, S. Lupi, J. Jiang, J. D. Weiss, E. E. Hellstrom, S. Lee, C. W. Bark, C. B. Eom, M. Putti, I. Pallecchi, and P. Dore, arXiv:1003.0565 (unpublished).
- ⁶² N. Barišić, D. Wu, M. Dressel, L. J. Li, G. H. Cao, and Z. A. Xu, Phys. Rev. B **82**, 054518 (2010).
- ⁶³ M. Dressel, D. Wu, N. Barišić, and B. Gorshunov, arXiv:1004.2962 (unpublished).
- ⁶⁴ A. Lucarelli, A. Dusza, F. Pfuner, P. Lerch, J. G. Analytis, J.-H. Chu, I. R. Fisher, and L. Degiorgi, New J. Phys. **12**, 073036 (2010).
- ⁶⁵ R. P. S. M. Lobo, Y. M. Dai, U. Nagel, T. Rõõm, J. P. Carbotte, T. Timusk, A. Forget, and D. Colson, arXiv:1007.3761 (unpublished).
- ⁶⁶ R. H. Liu, T. Wu, G. Wu, H. Chen, X. F. Wang, Y. L. Xie, J. J. Ying, X. J. Yan, Q. J. Li, B. C. Shi, W. S. Chu, Z. Y. Wu, and X. H. Chen, Nature (London) **459**, 64 (2009).
- ⁶⁷ P. M. Shirage, K. Kihou, K. Miyazawa, C.-H. Lee, H. Kito, H. Eisaki, T. Yanagisawa, Y. Tanaka, and A. Iyo, Phys. Rev. Lett. **103**, 257003 (2009).
- ⁶⁸ S. Raghu, X.-L. Qi, C.-X. Liu, D. J. Scalapino, and S.-C. Zhang, Phys. Rev. B **77**, 220503(R) (2008).
- ⁶⁹ D. J. Singh and M.-H. Du, Phys. Rev. Lett. **99**, 237003 (2008).
- ⁷⁰ D. J. Singh, Phys. Rev. B **78**, 094511 (2008).
- ⁷¹ I. I. Mazin, D. J. Singh, M. D. Johannes, and M. H. Du, Phys. Rev. Lett. **101**, 057003 (2008).
- ⁷² K. Kuroki, S. Onari, R. Arita, H. Usui, Y. Tanaka, H. Kontani, and H. Aoki, Phys. Rev. Lett. **101**, 087004 (2008).
- ⁷³ T. A. Maier and D. J. Scalapino, Phys. Rev. B **78**, 020514 (2008).
- ⁷⁴ A. V. Chubukov, D. V. Efremov, and I. Eremin, Phys. Rev. B **78**, 134512 (2008).
- ⁷⁵ A. V. Chubukov, M. G. Vavilov, and A. B. Vorontsov, Phys. Rev. B **80**, 140515(R) (2009).
- ⁷⁶ V. Mishra, G. Boyd, S. Graser, T. Maier, P. J. Hirschfeld, and D. J. Scalapino, Phys. Rev. B **79**, 094512 (2009).
- ⁷⁷ C. C. Homes, M. Reedyk, D. A. Cradles, and T. Timusk, Appl. Opt. **32**, 2976 (1993).
- ⁷⁸ M. Dressel and G. Grüner, *Electrodynamics of Solids* (Cambridge University Press, Cambridge, 2001).
- ⁷⁹ J. J. Tu, C. C. Homes, G. D. Gu, D. N. Basov, and M. Strongin, Phys. Rev. B **66**, 144514 (2002).
- ⁸⁰ A. Akrap, J. J. Tu, L. J. Li, G. H. Cao, Z. A. Xu, and C. C. Homes, Phys. Rev. B **80**, 180502(R) (2009).
- ⁸¹ M. Neupane, P. Richard, Y.-M. Xu, K. Nakayama, T. Sato, T. Takahashi, A. V. Fedorov, G. Xu, X. Dai, Z. Fang, Z. Wang, G.-F. Chen, N.-L. Wang, H.-H. Wen, and H. Ding, arXiv:1005.2966 (unpublished).
- ⁸² N. F. Mott, Phil. Mag **26**, 1015 (1972).
- ⁸³ M. Gurvitch, Phys. Rev. B **24**, 7404 (1981).
- ⁸⁴ N. E. Hussey, K. Takenaka, and H. Takagi, Phil. Mag. **84**, 2847 (2010).
- ⁸⁵ J. N. Hancock, S. I. Mirzaei, J. Gillett, S. E. Sebastian, J. Teyssier, R. Viennois, E. Giannini, and D. van der Marel, Phys. Rev. B **82**, 014523 (2010).
- ⁸⁶ R. A. Ferrell and R. E. Glover, III, Phys. Rev. **109**, 1398 (1958).
- ⁸⁷ M. Tinkham and R. A. Ferrell, Phys. Rev. Lett. **2**, 331 (1959).
- ⁸⁸ C. Jiang, E. Schachinger, J. P. Carbotte, D. Basov, and T. Timusk, Phys. Rev. B **54**, 1264 (1996).
- ⁸⁹ T. J. Williams, A. A. Aczel, E. Baggio-Saitovitch, S. L. Bud'ko, P. C. Canfield, J. P. Carlo, T. Goko, J. Munevar, N. Ni, Y. J. Uemura, W. Yu, and G. M. Luke, Phys. Rev. B **80**, 094501 (2009).
- ⁹⁰ R. T. Gordon, N. Ni, C. Martin, M. A. Tanatar, M. D. Vannette, H. Kim, G. D. Samolyuk, J. Schmalian, S. Nandi, A. Kreyssig, A. I. Goldman, J. Q. Yan, S. L. Bud'ko, P. C. Canfield, and R. Prozorov, Phys. Rev. Lett. **102**, 127004 (2009).
- ⁹¹ L. Luan, O. M. Auslaender, T. M. Lippman, C. W. Hicks, B. Kalisky, J.-H. Chu, J. G. Analytis, I. R. Fisher, J. R. Kirtley, and K. A. Moler, Phys. Rev. B **81**, 100501(R) (2010).
- ⁹² D. C. Mattis and J. Bardeen, Phys. Rev. **111**, 412 (1958).
- ⁹³ W. Zimmermann, E. Brandt, M. Bauer, E. Seider, and L. Genzel, Physica C **183**, 99 (1991).
- ⁹⁴ F. Massee, Y. Huang, R. Huisman, S. de Jong, J. B. Goedkoop, and M. S. Golden, Phys. Rev. B **79**, 220517(R) (2009).
- ⁹⁵ Y. H. Ren, M. Ebrahim, H. B. Zhao, G. Lüpke, Z. A. Xu, V. Adyam, and Q. Li, Phys. Rev. B **78**, 014408 (2008).
- ⁹⁶ E. E. M. Chia, J.-X. Zhu, D. Talbayev, R. D. Averitt, A. J. Taylor, K.-H. Oh, I.-S. Jo, and S.-I. Lee, Phys. Rev. Lett. **99**, 147008 (2007).
- ⁹⁷ A. Rothwarf and B. N. Taylor, Phys. Rev. Lett. **19**, 27 (1967).
- ⁹⁸ E. Grüneisen, Ann. Phys. (Leipzig) **16**, 530 (1933).
- ⁹⁹ M. Deutsch, J. Phys. A **20**, L811 (1987).
- ¹⁰⁰ Y. Kong, O. V. Dolgov, O. Jepsen, and O. K. Andersen, Phys. Rev. B **64**, 020501 (2001).
- ¹⁰¹ B. A. Mamedov and I. M. Askerov, Phys. Lett. A **362**, 324 (2007).
- ¹⁰² N. Ni, S. L. Bud'ko, A. Kreyssig, S. Nandi, G. E. Rustan, A. I. Goldman, S. Gupta, J. D. Corbett, A. Kracher, and P. C. Canfield, Phys. Rev. B **78**, 014507 (2008).
- ¹⁰³ J. W. Allen and J. C. Mikkelsen, Phys. Rev. B **15**, 2952 (1977).
- ¹⁰⁴ A. Puchkov, D. N. Basov, and T. Timusk, J. Phys.: Condens. Matter **8**, 10049 (1996).
- ¹⁰⁵ D. Wu, N. Barišić, M. Dressel, G. H. Cao, Z.-A. Xu, E. Schachinger, and J. P. Carbotte, Phys. Rev. B **82**, 144519 (2010).
- ¹⁰⁶ E. Schachinger, J. J. Tu, and J. P. Carbotte, Phys. Rev. B **67**, 214508 (2003).
- ¹⁰⁷ D. S. Inosov, J. T. Park, P. Bourges, D. L. Sun, Y. Sidis, A. Schneidewind, K. Hradil, D. Haug, C. T. Lin, B. Keimer, and V. Hinkov, Nature Phys. **6**, 178 (2010).
- ¹⁰⁸ T. Yildirim, Physica C **469**, 425 (2009).
- ¹⁰⁹ J. P. Carlo, Y. J. Uemura, T. Goko, G. J. MacDougall, J. A. Rodriguez, W. Yu, G. M. Luke, P. Dai, N. Shannon, S. Miyasaka, S. Suzuki, S. Tajima, G. F. Chen, W. Z. Hu, J. L. Luo, and N. L. Wang, Phys. Rev. Lett. **102**, 087001 (2009).
- ¹¹⁰ D. Wu, N. Barišić, N. Drichko, P. Kallina, A. Faridian, B. Gorshunov, M. Dressel, L. J. Li, X. Lin, G. H. Cao, and Z. A. Xu, Physica C In Press, Corrected Proof, (2009).
- ¹¹¹ C. C. Homes, A. Akrap, J. S. Wen, Z. J. Xu, Z. W. Lin, Q. Li, and G. D. Gu, Phys. Rev. B **81**, 180508(R) (2010).
- ¹¹² C. C. Homes, S. V. Dordevic, M. Strongin, D. A. Bonn, R. Liang, W. N. Hardy, S. Komiyama, Y. Ando, G. Yu, N. Kaneko, X. Zhao, M. Greven, D. N. Basov, and T. Timusk, Nature (London) **430**, 539 (2004).
- ¹¹³ C. C. Homes, S. V. Dordevic, T. Valla, and M. Strongin, Phys. Rev. B **72**, 134517 (2005).